

Bacterially mediated mineralization of vaterite

Carlos Rodriguez-Navarro ^{a,*}, Concepcion Jimenez-Lopez ^b, Alejandro Rodriguez-Navarro ^a,
Maria Teresa Gonzalez-Muñoz ^b, Manuel Rodriguez-Gallego ^a

^a Departamento de Mineralogía y Petrología, Universidad de Granada, Fuentenueva s/n, 18002 Granada, Spain

^b Departamento de Microbiología, Universidad de Granada, Fuentenueva s/n, 18002 Granada, Spain

Received 4 May 2006; accepted in revised form 27 November 2006

Abstract

Myxococcus xanthus, a common soil bacterium, plays an active role in the formation of spheroidal vaterite. Bacterial production of CO₂ and NH₃ and the transformation of the NH₃ to NH₄⁺ and OH⁻, thus increasing solution pH and carbonate alkalinity, set the physicochemical conditions (high supersaturation) leading to vaterite precipitation in the microenvironment around cells, and directly onto the surface of bacterial cells. In the latter case, fossilization of bacteria occurs. Vaterite crystals formed by aggregation of oriented nanocrystals with *c*-axis normal to the bacterial cell-wall, or to the core of the spherulite when bacteria were not encapsulated. While preferred orientation of vaterite *c*-axis appears to be determined by electrostatic affinity (ionotropic effect) between vaterite crystal (0001) planes and the negatively charged functional groups of organic molecules on the bacterium cell-wall or on extracellular polymeric substances (EPS), analysis of the changes in the culture medium chemistry as well as high resolution transmission electron microscopy (HRTEM) observations point to polymorph selection by physicochemical (kinetic) factors (high supersaturation) and stabilization by organics, both connected with bacterial activity. The latter is in agreement with inorganic precipitation of vaterite induced by NH₃ and CO₂ addition in the protein-rich sterile culture medium. Our results as well as recent studies on vaterite precipitation in the presence of different types of bacteria suggest that bacterially mediated vaterite precipitation is not strain-specific, and could be more common than previously thought.

© 2006 Elsevier Inc. All rights reserved.

1. Introduction

Bacterially induced or mediated carbonate mineralization is thought to be important in a range of processes including atmospheric CO₂ budgeting (Braissant et al., 2002; Ehrlich, 2002), carbonate sediment and rock formation (Riding, 2000; Ben Chekroun et al., 2004), biogeochemical cycling of elements (Banfield and Nealson, 1997; Ehrlich, 2002), metal-contaminated groundwater bioremediation (Warren et al., 2001; Fujita et al., 2004; Mitchell and Ferris, 2005, 2006) and conservation of ornamental stone (Rodriguez-Navarro et al., 2003). Calcite and aragonite are the most common microbial carbonates (Ehrlich, 2002). Interestingly, microbial biscuits of vaterite, the rare

metastable CaCO₃ polymorph (Lippmann, 1973), have been found in a lake (Giralt et al., 2001), while *in vitro* bacterially mediated vaterite precipitation has also been reported (Rivadeneira et al., 1991; Groth et al., 2001; Warren et al., 2001; Braissant et al., 2002, 2003; Cacchio et al., 2003; Rodriguez-Navarro et al., 2003; Hammes et al., 2003; Sanchez-Moral et al., 2003; Ben Chekroun et al., 2004; Rivadeneira et al., 2006). These occurrences suggest that bacterial vaterite precipitation is more common than previously thought. Nonetheless, it is not fully understood how bacteria induce or mediate the formation of such an unusual CaCO₃ polymorph (Lippmann, 1973). Although it is well established that calcium carbonate polymorph selection and crystal orientation in higher organisms such as bivalves is biologically controlled (Belcher et al., 1996; Falini et al., 1996), it is unknown whether such remarkable control exists in prokaryotes. Elucidating how bacterial vaterite mineralization occurs may have far reaching

* Corresponding author.

E-mail address: carlosrn@ugr.es (C. Rodriguez-Navarro).

implications: it may lead to a better understanding of microbial carbonate mineralization, and help identify bio-signatures both on Earth and elsewhere. Furthermore, it may shed light on the “calcium carbonate polymorphism problem”, which is one of the biggest challenges in the field of biomineralization (Falini et al., 2005).

Vaterite typically precipitates in a spherical shape when grown in the laboratory from highly supersaturated and moderately alkaline solutions (Ogino et al., 1987; Kralj et al., 1997; Vecht and Ireland, 2000). It has a hexagonal structure (Meyer, 1969) and it is unstable under practically all known conditions (Friedman et al., 1993). The latter is caused by the higher solubility (Plummer and Busenberg, 1982) and lower density of vaterite as compared to those of calcite and aragonite (Lippmann, 1973). In aqueous solution vaterite rapidly transforms into one of the latter phases (Kralj et al., 1997; Spanos and Koutsoukos, 1998). Only at 1 atm pressure and $T \leq 10^\circ\text{C}$ has vaterite been described as a stable phase of CaCO_3 (Albright, 1971). Nonetheless, it appears that for reasons yet unknown vaterite is more stable than previously thought (Friedman et al., 1993).

In nature vaterite has been found in calcareous sediments (Benton et al., 1963), metamorphic rocks (McConnell, 1960) and drilling muds (Friedman and Schultz, 1994). It has also been found in portland cement (Cole and Kroone, 1959), ancient plasters (ca. 700 BC) of the Siloam Tunnel, Jerusalem (Frumkin et al., 2003) and in mortars of the Florence Cathedral (Signorelli et al., 1996). DuFresne and Anders (1962) reported vaterite presence in Pesyanoe meteorite, although it was unclear whether it was terrestrial or antecedent in origin. Despite such occurrences, some controversy exists regarding whether vaterite can precipitate inorganically from natural waters (Lucas and Andrews, 1996). Nonetheless, inorganic vaterite precipitation in the Canadian Arctic has been recently reported (Grasby, 2003).

Most natural occurrences of vaterite are associated with biogenic activity (Lippmann, 1973; Lowenstam and Weiner, 1989; Mann, 2001). This is the case for abnormally calcified tissues, including regenerated damaged gastropod shells (Mayer and Weineck, 1932) and human pathological concretions such as gallstones (Sutor and Wooley, 1968; Bassi et al., 1994; Bogren et al., 1995; Palchik and Moroz, 2005), pancreatic stones and cloggings in human heart valves (Kanakis et al., 2001). Vaterite is sometimes found in hard tissues of some marine organisms (Lowenstam and Abbott, 1975), egg-shells of gastropods (Hall and Taylor, 1971) and birds (Dennis et al., 1996), vertebrate otoconia (Wright et al., 1982), crustacean statoliths (Ariani et al., 1993), and fish otoliths (David et al., 1994; Oliveira et al., 1996; Falini et al., 2005).

The presence of organic molecules associated with living organisms seems to aid vaterite formation and/or stabilization. In fact, *in vitro* precipitation of vaterite is generally favored over more stable calcite and aragonite when organic macromolecules are present (Mann et al., 1988, 1991;

Rajam et al., 1991; Falini et al., 1998, 2000; Mann, 2001; Naka and Chujo, 2001). Vaterite precipitation is promoted by organic polymeric substances (Naka and Chujo, 2001), particularly those including carboxylic groups (Dalas et al., 1999; Agarwal and Berglund, 2003; Braissant et al., 2003; Ichikawa et al., 2003; Tong et al., 2004; Grassmann and Löbmann, 2004; Malkaj and Dalas, 2004), phosphonates (Dupont et al., 1997; Sawada, 1997), sulfonates (Jada and Verraes, 2003), and amino acids (Manoli et al., 2002; Xie et al., 2005). Surfactants (anionic) also induce vaterite formation (Walsh et al., 1999; Shen et al., 2005a). Besides the typical spheroidal structure (Cölfen and Antonietti, 1998), organics also induce *in vitro* precipitation of vaterite structures with a variety of complex shapes: e.g., dumbbell (Cölfen and Qi, 2001), fried-egg and flowerlike (Rudolf and Cölfen, 2003; Liang et al., 2004), torus and spongelike (Walsh et al., 1999), lenticular (Gehrke et al., 2005), plate-like (Dupont et al., 1997), cakelike (Chen et al., 2006), and wirelike (Balz et al., 2005).

However, the role of organic molecules on vaterite growth and stabilization is still controversial. Basically, two explanations have been suggested for organics-induced vaterite precipitation/stabilization: (a) organics act as a template for vaterite heterogeneous nucleation (Mann et al., 1988; Mann, 2001), and (b) organic molecules inhibit the transition from metastable to stable phases (Sawada, 1997; Xu et al., 2004; Lakshminarayanan et al., 2005). In the first case, a structural matching between the organic molecules and specific (*hkil*) planes of vaterite leads to the heterogeneous crystallization (epitaxy) of this metastable phase (Mann, 2001). In the second case, the Ostwald step sequence is stopped at one of its intermediate stages: i.e., amorphous calcium carbonate (ACC) \rightarrow vaterite \rightarrow calcite (Ogino et al., 1987; Clarkson et al., 1992; Jimenez-Lopez et al., 2001). The large number of organic molecules, with very different structures, that reportedly induce vaterite precipitation (Naka and Chujo, 2001) is not fully consistent with the template model proposed by Mann (2001). Conversely, the formation of oriented vaterite on a variety of organic monolayers (Mann et al., 1988) and organic matrices (Falini et al., 1998) supports Mann's model. However, DiMasi et al. (2003) have shown that vaterite formation under organic monolayers is not template-directed; rather, it is controlled by kinetic effects. It follows that a definitive model which explains how vaterite forms in contexts relevant to biomimetic mineralization and/or biomineralization is still lacking.

Vaterite precipitated in the presence of bacteria typically appears as micron-sized spherulites (Ben Chekroun et al., 2004). It has been suggested that vaterite spherules, with strong similarities to vaterite formed in the presence of bacteria, could be a precursor of the carbonates found in Martian meteorite ALH84001 (Vecht and Ireland, 2000). This suggestion could have important implications in the search for evidence of past biogenic activity in Mars. However, most typical morphologies of bacterial carbonates, including single crystals, dumbbells, crystal bundles, and

spherulites, have been precipitated abiotically (Ben Cherkroun et al., 2004). In particular, abiotic vaterite typically forms micron-sized spherulites (solid or hollow) made up of fibrous-radiate crystals (Cölfen and Antonietti, 1998; Vecht and Ireland, 2000). Furthermore, vaterite with worm-like morphologies very similar to that of the putative bacterial carbonates in ALH84001 meteorite have been produced abiotically in the absence of organics (Fan and Wang, 2005). The recognition of bacterial biosignatures based on purely morphological considerations is therefore very difficult.

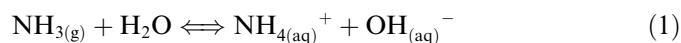
This study shows that *Myxococcus xanthus*, a common soil bacterium, mediates the formation of accretionary vaterite structures. The analysis of the evolution of the chemistry in the bacterial culture medium and the ultra-structure of vaterite spherulites help disclose how this CaCO₃ phase forms. Furthermore, the accretionary nature of the vaterite structures (i.e., characterized by successive concentric shells), offers important information about the life history of (bio)mineralization events and the chemical evolution of the crystallization environment. Ultimately, this study suggests that the micro- and nano-structure of biotic vaterite structures may help identify bacterial activity in a range of environments expanding from pathological concretions to the geological record.

2. Materials and methods

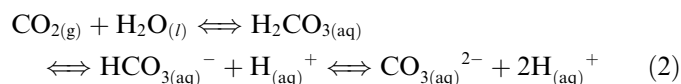
2.1. Bacterial strain

Myxococcus xanthus (strain number 422; Spanish Type Culture Collection, Burjasot, Spain) was used for CaCO₃ mineralization. *M. xanthus* is an abundant and ubiquitous Gram-negative, non-pathogenic heterotrophic soil bacterium, which belongs to the δ -subdivision of the Proteobacteria (Dworkin and Kaiser, 1993). It has been selected because it displays a remarkable capacity to induce/mediate the precipitation of different mineral phases (Ben Cherkroun et al., 2004), including carbonates, sulfates and phosphates (Ben Omar et al., 1994; González-Muñoz et al., 1996, 2000, 2003).

Regarding its ability to mediate the formation of carbonates, *M. xanthus* metabolism results in the release CO₂ and NH₃ (Rodríguez-Navarro et al., 2003). Ammonia release increases the pH in the culture medium according to the equilibrium:



The increase in pH leads to a rise in the concentration of CO_{3(aq)}²⁻ in the culture medium, as indicated by the following equilibria:



In the presence of Ca_(aq), at some point the culture medium becomes supersaturated with respect to a particular calci-

um carbonate phase (calcite, aragonite or vaterite), leading to its precipitation according to the following equilibrium:



2.2. Culturing of *M. xanthus* cells and biotic precipitation experiments

Inocula were prepared by cultivating *M. xanthus* in test tubes containing 5 ml/tube CT medium (Dworkin and Kaiser, 1993). Test tubes were incubated for 48 h at 28 °C with constant shaking (180 rpm; Gallenkamp rotary shaker) up to a cell density of $\sim 2 \times 10^9$ cells/ml. Production of CaCO₃ occurred in inoculated M-3 medium (Rodríguez-Navarro et al., 2003). M-3 liquid medium was prepared by mixing (values in wt/vol) 1% Bacto Casitone (pancreatic digest of casein; Difco), 1% Ca(CH₃OO)₂·4H₂O, and 0.2% K₂CO₃·1/2H₂O (pH 8). Fifteen 250 ml Erlenmeyer flasks were filled with 100 ml of M-3 medium and sterilized by autoclaving for 20 min at 120 °C. Eight Erlenmeyer flasks were inoculated with 2 ml of the bacterial inoculum. The remaining seven Erlenmeyer flasks were not inoculated (negative biotic controls). All Erlenmeyer flasks were incubated at 28 °C with constant shaking (67 rpm; Braun rotary Certomat-R) for different time lengths: 0, 1, 3, 5, 7, 10, 15, and 30 days. Porous Pyrex glass disks (10 mm diameter, 5 mm thickness; Bibby Sterling Ltd.) were placed in a set of Erlenmeyer flasks inoculated and non-inoculated (i.e., negative biotic controls) as support for mineral precipitation in order to prepare thin sections for transmission electron microscopy (TEM) analysis.

2.3. Abiotic precipitation experiments

Carbonate precipitation tests were performed in the absence of bacteria to serve as abiotic (chemical) controls (as in Ferris et al., 2003). Sterile M-3 medium with and without Bacto Casitone was poured in 20 ml test tubes (twelve test tubes, each half-filled with 10 ml solution). The pH of the solution was then adjusted to the target pH by adding NH₃(l) (from pH 8 up to pH 10.6), thus mimicking *M. xanthus* metabolic activity. No precipitation took place following pH rise within the time scale of the biotic experiment, i.e., 30 days. Precipitation was thus induced by bubbling CO₂ into the solution at a flow rate of 10 ml/min (up to 2 min). After ~ 1 min of CO₂ bubbling, a white precipitate formed. Aliquots (0.5 ml) were pipetted right after the first precipitates were formed, transferred to glass slides and observed on a polarized-light microscope. The same operation was performed 1 h after the onset of precipitation. Precipitates were aged for 48 h in the mother liquor. Following sedimentation, the supernatant solution was decanted, and the solids were collected, rinsed several times

with distilled water, and dried in an oven at 60 °C for 4 h before further analysis.

2.4. Sampling and analysis

Changes in the chemistry of the medium due to bacterial metabolism were studied by monitoring the evolution over time of pH, total aqueous calcium concentration, $\text{Ca}_{\text{T(aq)}}$, and supersaturation with respect to vaterite, Ω_{vaterite} . At predetermined time intervals, two Erlenmeyer flasks (inoculated and uninoculated control) were opened and 20 ml of liquid sample were withdrawn for pH, $\text{Ca}_{\text{T(aq)}}$ and $\text{NH}_{3(\text{aq})}$ analysis. Solutions were filtered (0.1 μm Millipore membrane) and pH was measured (combination pH electrode, Crison). Experimental error for pH measurements was ± 0.05 (1σ). $\text{Ca}_{\text{T(aq)}}$ was determined by atomic absorption spectrophotometry (AAS, Perkin-Elmer 1100B) using an air–acetylene flame atomizer, after acidification of samples with HCl to prevent further precipitation of solid carbonate. Experimental error for $\text{Ca}_{(\text{aq})}$ was ± 0.05 mM (1σ). $\text{NH}_{3(\text{aq})}$ concentration in the culture medium was measured using the HACH DR 850 colorimeter and the Salicylate method. Based on repeated measurements, experimental error for $\text{NH}_{3(\text{aq})}$ was 0.05 mM (1σ).

Solution in the Erlenmeyer flasks was centrifuged at the end of the experiment and the solid was collected and rinsed several times with distilled water to eliminate the nutritive solution and the remaining cellular debris. Further washing with ethanol was performed prior to thermal analysis to ensure that organics (not included within the carbonate precipitates) were fully eliminated. Washing with ethanol was performed up to four times.

The mineralogy of both biotic and abiotic precipitates was determined by powder X-ray diffraction (XRD) using a Philips PW-1710 diffractometer (Cu $K\alpha$ radiation, $\lambda = 1.5405$ Å; exploration range, 2θ , 20°–60°; steps of 0.02° 2θ ; goniometer speed of 0.005° 2θ s^{-1}). Vaterite crystallite size, D_{hkl} , was calculated using the Scherrer equation (Klug and Alexander, 1954). Fourier transform infrared spectroscopy (FTIR) of both biotic and abiotic precipitates was performed on a Nicolet 20SXB with a resolution of 0.5 cm^{-1} . Prior to FTIR analysis, precipitates were pressed into KBr pellets. FTIR analyses were performed to identify the CaCO_3 polymorph and the presence of organic macromolecules within the CaCO_3 structure. Thermogravimetric (TGA) analysis of biotic and abiotic precipitates was performed on a Shimadzu TGA-50H coupled with a Nicolet 550 FTIR spectrometer for evolved gas analysis. Differential scanning calorimetry (DSC) analysis of biotic precipitates was carried out on a Shimadzu DSC-50Q. Thermal analyses were performed to elucidate (and quantify) whether or not organic matter was incorporated into carbonate precipitates. Samples (~40 mg) were placed in Al sample holders and analyzed in air at a heating rate of 20 °C min^{-1} from room T up to 450 °C (DSC) or up to 950 °C (TGA).

Morphology of the biotic and abiotic precipitates was studied using a field emission scanning electron microscope

(FESEM; Leo Gemini 1530). Precipitates were placed on sticky carbon-coated stubs attached to Al sample holders. Samples were C coated. No further preservation or fixation treatment was performed before FESEM observation. Carbonates formed right after the onset of crystallization in abiotic tests were observed using a polarized-light optical microscope (C. Zeiss mod. Jenapol-U).

Canadian balsam-mounted thin sections of mineralized porous glass supports (biotic tests) were prepared and polished. Following a preliminary optical microscopy analysis, carbonates were studied using a TEM (Philips CM20) operated at a 200 kV. The objective aperture was 40 μm , which is a compromise between amplitude and phase contrast images. Prior to TEM observations, the selected carbonates were glued to Cu rings, removed from the thin sections, further thinned using a Gatan 600 ion-mill and, finally, carbon-coated. Another set of both biotic and abiotic precipitates (powdery samples) were dispersed in ethanol and deposited on carbon-coated Cu grids before TEM observations. The elemental composition of precipitates was determined by means of energy-dispersive X-ray spectroscopy, EDS (EDAX detector with ultrathin-window coupled to the TEM). Spot analyses were performed on different areas of the carbonate structures.

2.5. Calculations

Activities and activity coefficients for all aqueous species were calculated using the EQ3/6 program (Wolery, 1992) from measured values of $\text{Ca}_{\text{T(aq)}}$, pH, and $\text{NH}_{3(\text{aq})}$ and calculated values of alkalinity, acetate and $\text{K}^{(\text{aq})}$ (24.2 mM). The amount of acetate was assumed to vary within a maximum of 5% of the initial amount, since it has not been described in the literature that *M. xanthus* uses or produces any significant extracellular acetate. In the case of the non-inoculated biotic tests (negative biotic control), the concentration of acetate over time was considered constant and equal to that at the beginning of the experiment (120.6 mM). To properly determine the saturation value with respect to a particular phase of calcium carbonate, it is necessary to determine $\text{Ca}_{\text{T(aq)}}$ and two out of the four following parameters: TCO_2 (total dissolved carbon), P_{CO_2} (CO_2 pressure), alkalinity and pH. Because P_{CO_2} could not be measured in our experiments, it was chosen to determine pH and alkalinity. To properly measure P_{CO_2} it would have been necessary to use a closed system to perform the experiments. However, since *M. xanthus* is an aerobic bacterium and the experiments were run for long periods of time (1 month), the use of a closed system was not possible, because cutting out the oxygen supply could have limited the growth of such bacterium. It was not possible to measure carbonate alkalinity either, because the acetate ion (present in the culture medium) acted as a buffer thus preventing the use of acid-titration methods. Therefore, alkalinity had to be calculated. Carbonate alkalinity and acetate concentration at each time interval were adjusted by means of charge balance, which was based on

the measured pH and concentrations of the ionic species in solution: calcium, ammonium, potassium and acetate. Such charge balance is performed by EQ3/6 as follows: the program calculates possible charge imbalances (due to an incorrect value of alkalinity) and corrects them by adjusting the proton concentration. Such correction yields an output pH value that is different than the input pH value due to an incorrect input value for the carbonate alkalinity. Therefore, when the pH calculated by the program is equal to the measured pH, the solution charge is balanced and, as a consequence, the input alkalinity value is correct. Errors in the data calculated by this method are based on the analytical errors associated to measured parameters, and resulted in a variation of $\pm 10\%$ of saturation values. Nevertheless, the focus of this study is not on the specific values of saturation at which phenomena occur, but rather on saturation trends throughout the experiment. Even though the saturation value at a certain time could be 10% higher or lower, the observed trends remain unaltered.

Ion activity products (IAP) at each time interval were calculated as the product of the activity of calcium and carbonate in solution ($a_{\text{Ca}} \times a_{\text{CO}_3^{2-}}$). Saturation state (Ω) with respect to the particular CaCO_3 phase is defined as: $\Omega = \text{IAP}/K_{\text{sp}}$, where IAP is the ionic activity product and K_{sp} is the solubility product for the relevant mineral phase ($\text{p}K_{\text{ps,vaterite}} = 7.913$, $\text{p}K_{\text{ps,aragonite}} = 8.34$ and $\text{p}K_{\text{ps,calcite}} = 8.48$; Plummer and Busenberg, 1982).

3. Results and discussion

3.1. Biotic and abiotic vaterite precipitation

Vaterite was precipitated in liquid medium M-3 inoculated with *M. xanthus*, as confirmed by XRD analysis (Fig. 1a). No precipitation took place in the negative biotic

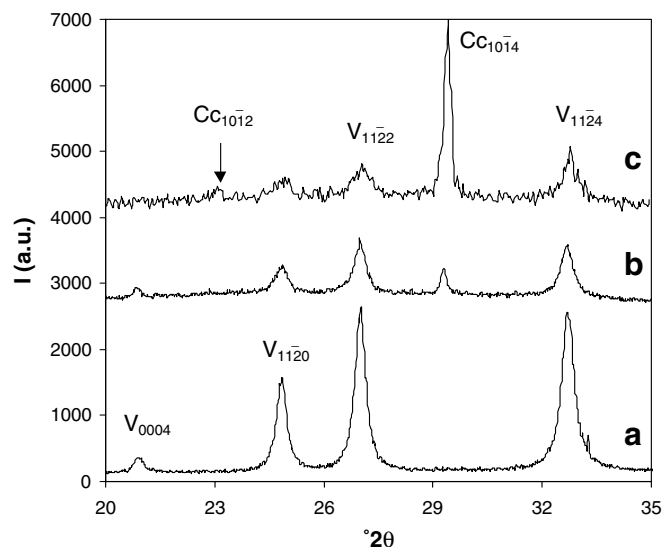


Fig. 1. XRD patterns of carbonates. Biotic vaterite (a), and abiotic carbonates in samples collected 1 h (b) and 48 h (c) after the onset of precipitation. *hkl* values of Bragg peaks are indicated (Cu $K\alpha$ radiation, $\lambda = 1.5405 \text{ \AA}$). V, vaterite; Cc, calcite.

controls. XRD analysis of abiotic precipitates showed that calcite and vaterite formed in the presence of Bacto Casitone (Fig. 1b–c). In the latter case, vaterite was present in concentrations ranging from 50 ± 5 up to 85 ± 5 wt%, calculated from XRD results according to the method proposed by Dickinson and McGrath (2001). The highest amount, 85 ± 5 wt%, was observed one hour after the onset of precipitation (Fig. 1b), and dropped to 50 ± 5 wt% when abiotic vaterite was kept in contact with the solution for 48 h (Fig. 1c). Calcite was the only phase detected by XRD following abiotic carbonate precipitation in the absence of Bacto Casitone. Abiotic precipitation occurred following CO_2 bubbling, only when the initial pH of the solution was artificially raised above pH 10.

Optical microscopy analysis of abiotic precipitates formed in the absence of Bacto Casitone showed the formation of rhombohedral crystals (calcite). At the onset of carbonate precipitation in the presence of Bacto Casitone, birefringent micron-sized spherulites (i.e., vaterite) formed. A reduction in the amount of spherulitic precipitates was observed one hour after the onset of precipitation, when the new formation of rhombohedral precipitates (calcite) occurred. The results of the abiotic experiments show that the presence of organics (and a high supersaturation) are necessary for vaterite formation and (partial) stabilization. These observations are fully consistent with earlier reports on the formation and transformation of vaterite (e.g., Ogino et al., 1987; Clarkson et al., 1992; Sawada, 1997; Han et al., 2006).

FTIR spectra of biotic and abiotic carbonates are shown in Fig. 2. The characteristic peaks of calcite at 714 (ν_4), 876 (ν_2), and 1420 (ν_3) cm^{-1} (Fig. 2c) were detected in all the abiotic experiments (Fig. 2b). The distinctive vaterite absorption bands at 745 and 1085 cm^{-1} (Dupont et al., 1997) were detected in the abiotic (with Bacto Casitone) and biotic precipitates (Fig. 2a and b). Biotic precipitates did not show the distinctive calcite peak at 714 cm^{-1} . These observations are consistent with XRD results.

Interestingly, FTIR spectra of biotic vaterite and abiotic carbonates formed in the presence of Bacto Casitone showed additional absorption bands that do not correspond to carbonate phases. The presence of proteins was indicated by the amide I signature at 1655 cm^{-1} (Rautaray et al., 2003). Amino acids in Bacto Casitone account for the amide shoulder in the abiotic precipitates. This shoulder is much better defined in the biotic vaterite, which suggests that it incorporates a larger amount of amino acids. Using FTIR, Sondi and Matijević (2001) also detected proteins in vaterite formed by urease catalyzed reaction. Ueyama et al. (2002) and Takahashi et al. (2004) have reported that tight binding between amide groups and vaterite surface via $\text{NH}\cdots\text{O}$ hydrogen bonds controls CaCO_3 polymorph selection and the long-term stabilization of vaterite. Other adsorption bands were detected in biotic vaterite: a small broad hump at 1100 cm^{-1} corresponding to sugar (Aizenberg et al., 2002); and other organic matter absorption bands such as those of the carboxylic group at

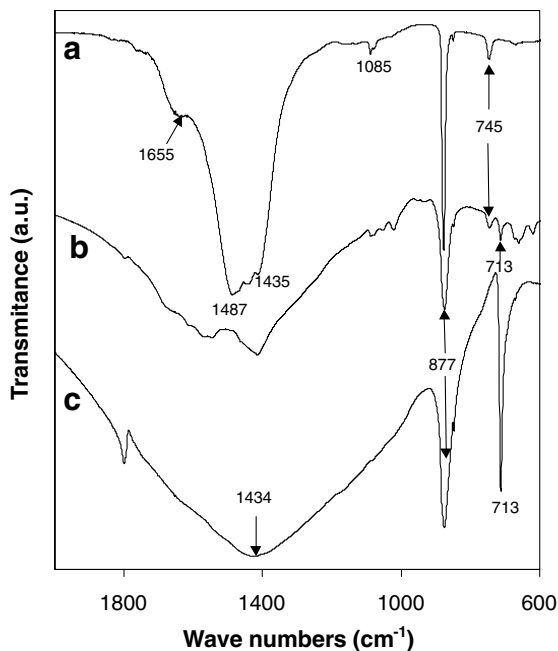


Fig. 2. FTIR spectra of biotic vaterite (a), abiotic carbonates formed in the presence of Bacto Casitone (b), and abiotic calcite formed in the absence of Bacto Casitone (c).

1560 and 1360 cm^{-1} (Williams and Fleming, 1989), which could not be unambiguously identified because they were partially masked by the strongest band of the carbonate group at 1420 cm^{-1} . It is worth mentioning that bacterial activity induces the formation of significant amounts of extracellular polymeric substances (EPS) that typically surround the bacterial cells forming biofilms (Decho, 2000). EPS has been shown to be a rich matrix of polymers, including polysaccharides, proteins, glycoproteins, nucleic acids, phospholipids, and humic acids (Beveridge and Graham, 1991; Wingender et al., 1999; McSwain et al., 2005). In particular, polymerized amino sugars, e.g., chitin, have been found in *M. xanthus* EPS (Li et al., 2003). Chitin is well known for its capacity to induce vaterite precipitation (Falini et al., 2002). In summary, our FTIR results show that organic by-products of bacterial activity, in addition to amino acids in the culture broth, are incorporated into the biotic vaterite structures.

DSC analysis shows that decomposition of organics within biotic and abiotic carbonates took place in the T range of 150–500 °C, with an exothermal peak at 317–328 °C (Fig. 3). A small endothermal peak was detected at $T < 150$ °C, which was assigned to (adsorbed) H_2O loss (ca. 3% weight loss, according to TGA analysis). Thermal decomposition of organics resulted in the release of CO , CO_2 , and NO_2 that were detected by on-line FTIR spectrometry of evolved gases. NH_3 was also released following thermal decomposition of biotic vaterite. The composition of evolved gases corroborates that amino acids (among other organic molecules) are included within the carbonates. TGA results showed that up to 16.7 and 5.8 wt% organic matter was present in the biotic vaterite and abiotic

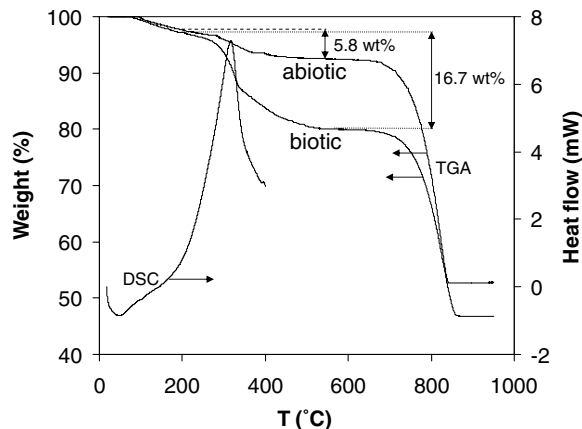


Fig. 3. DSC/TGA curves of biotic vaterite and abiotic carbonates formed in the presence of Bacto Casitone. Weight loss due to organics decomposition (150–500 °C) is indicated. Note that the largest weight loss (650–850 °C) is due to thermal decomposition of CaCO_3 .

carbonates, respectively (Fig. 3). Incorporation of organic species in biomimetic calcite and vaterite has been reported (Grassmann et al., 2002, 2003; Wang et al., 2003; Shen et al., 2005b). Considering that vaterite density is 2.65 g/cm^3 (Lippmann, 1973) and assuming a density of ~ 1.3 g/cm^3 for the organics (Grassmann et al., 2002), it can be estimated that the biotic precipitates contain about 30 vol% organic matter. This value is consistent with quantitative digital image analysis of low-electron absorbing areas in low-resolution TEM images of biotic vaterite structures (Figs. 7D and 8C), which yields values of 25 ± 10 vol% organic matter. The significantly lower amount of organic matter in abiotic precipitates may account for their lower stability (i.e., XRD and optical microscopy results showing transformation of abiotic vaterite into calcite over time). In contrast biotic vaterite crystals were preserved after more than 30 days in the culture medium and, at least, 2 years storage in the laboratory (20 °C and 55% relative humidity).

FESEM analyses revealed that biotic precipitates were spherulites, 0.5–5 μm in diameter (Fig. 4a and b). Scarce rod-shaped bacterial cells (with length ca. 2 μm and a diameter of ca. 0.5 μm) were also observed (Fig. 4c). Such bacterial cells were surrounded by nanometer-sized carbonate crystals. Some vaterite spherulites encapsulated bacterial cells. Their cross-section could be seen in broken spherulites (Fig. 4d), and consisted of two concentric mineral rings. Vaterite crystal morphology and size changed across the shell thickness. Crystals increased their size towards the shell outer surface. The presence of vaterite spherulites with diameters smaller than that of the typical bacterial cells length (ca. 2 μm) suggests that many of the vaterite spherulites do not encapsulate bacteria. It therefore appears that the presence of bacterial cells is not a prerequisite for the formation of the vaterite spherulites. Nonetheless, bacterial activity seems to be a prerequisite for their formation, since no precipitation occurred in the negative biotic controls.

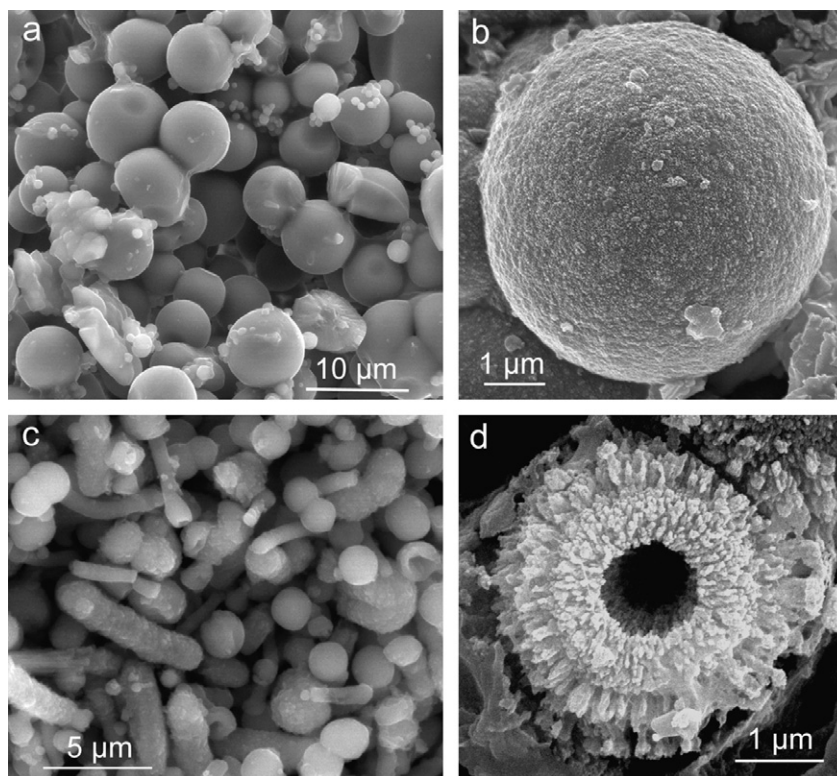


Fig. 4. FESEM photomicrographs of biotic vaterite structures: (a) general overview of vaterite spherulites; (b) detail of a vaterite spherulite; its surface is rough (at a nanometer scale) due to the end-points of carbonate crystals (best observed in a cross-section); (c) detail of vaterite spherulites and calcified rod-shaped bacterial cells; and (d) cross-section of vaterite hollow spherulite showing the empty nucleus where the bacterium was located; two concentric rings are observed with marked differences in crystal size and density.

FESEM analysis of abiotic carbonates formed in the absence of Bacto Casitone revealed the presence of well-developed rhombohedral calcite crystals (Fig. 5A). Vaterite spherulites and aggregates with morphologies and sizes that were very similar to those of biotic vaterite spherulites formed in the presence of Bacto Casitone (Fig. 5B). Some abiotic vaterite structures revealed the presence of rhombohedral nanocrystals at the sphere surface, while other spheres showed poorly developed rhombohedral faces (Fig. 5C). Rhombohedral calcite crystals were also observed (Fig. 5D). These observations suggest that many vaterite spherulites are partially or totally transformed into calcite aggregates or rhombohedra. These observations are consistent with optical microscopy and XRD results showing transformation over time of vaterite into calcite.

From these observations it follows that the morphological features of vaterite spherulites can not be unambiguously used to identify biosignatures of bacterial activity, since they can be obtained abiotically too. On the other hand, the presence of organics seems to be crucial for the formation and stabilization of such vaterite structures.

3.2. Evolution of bacterial culture chemistry

Bacterial activity was not identical in each set of experiments, resulting in variations in the measured parameters at a certain time period for the three replicas. However,

the trends remained unaltered. Therefore, we present the results of a representative experiment.

Myxococcus xanthus metabolic activity results in CO₂ and NH₃ release (Table 1). While CO₂ contributes to a reduction in pH, ammonia release increases pH. The latter effect outcomes the former, as shown by the continuous increase in pH over the time course of the biotic test experiments (Fig. 6a). The precipitation of calcium carbonate reduces both pH and total calcium in solution, Ca_{T(aq)}. The Ca_{T(aq)} also decreases most probably because of Ca adsorption at negatively charged sites on the bacterium cell walls (Schultze-Lam et al., 1996). Limited Ca adsorption onto the glass walls of the Erlenmeyer flasks is not ruled out (see below). Calcium carbonate precipitation can be followed by recording the evolution over time of the supersaturation of the culture medium. This evolution is also directly related to bacterial metabolism. Supersaturation values rise as a consequence of increases in pH and alkalinity induced by bacterial metabolism. Supersaturation values decrease when calcium, carbonate and/or pH become lower due to the precipitation of calcium carbonate. According to our results (Fig. 6b and c), supersaturation values rise within the first stages of the experiment (first week) and within the time period 10–15 days. Bacterial activity increased Ω_{vaterite} to a maximum value well above that of the negative biotic control test experiment (89.7 vs. 48.7), thus inducing the precipitation of vaterite. Such

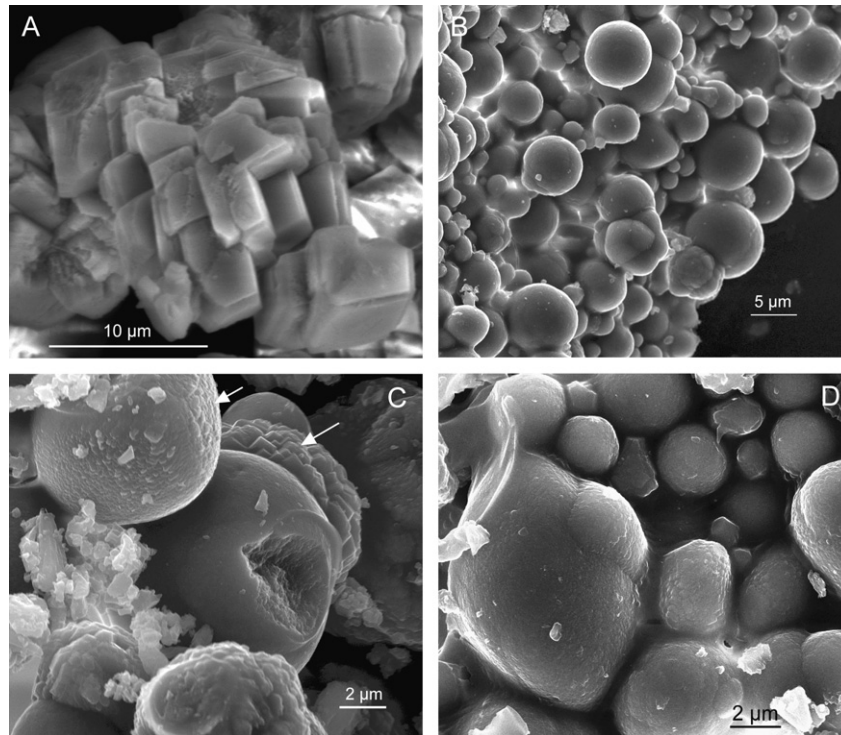


Fig. 5. FESEM photomicrographs of abiotic carbonates: (A) calcite aggregates formed in the absence of Bacto Casitone; (B) general overview of vaterite spherulites formed in the presence of Bacto Casitone; (C) detail of vaterite spherulites with rhombohedral crystal faces at their surface (arrows); and (D) detail of a rhombohedral calcite crystal surrounded by vaterite spherulites.

Table 1

Measured pH, total calcium ($\text{Ca}_{\text{T(aq)}}$) and ammonium ($\text{NH}_{3(\text{aq})}$) in solution; calculated alkalinity, calcium and carbonate activity, ionic activity product (IAP) and supersaturation of the system with respect to vaterite

Time (days)	pH	$\text{Ca}_{\text{T(aq)}} \text{ (mM)}$	$\text{NH}_{3(\text{aq})} \text{ (mM)}$	Alkalinity (mM)	$\log a\text{Ca}^{2+}$	$\log a\text{CO}_3^{2-}$	IAP	Ω_{vaterite}
<i>Run type: M-3 (negative biotic control)</i>								
0	8.00	52.5	1.81	15.6	-1.9772	-4.3341	4.88E-07	40.0
1	8.03	45.3	0.43	9.4	-2.0151	-4.4165	3.70E-07	30.3
3	8.03	47.3	0.35	13.3	-2.0234	-5.0351	8.74E-08	7.2
5	8.01	49.1	0.72	14.3	-2.0461	-4.2354	5.23E-07	42.8
7	7.98	50.9	0.21	13.8	-1.9714	-4.2544	5.95E-07	48.7
10	8.05	50.5	0.90	14.1	-2.1101	-4.1847	5.07E-07	41.5
15	8.04	50.1	0.44	14.2	-2.1439	-4.1847	4.69E-07	38.4
30	8.07	50.2	0.62	14.0	-1.9770	-4.2725	5.63E-07	46.1
<i>Run type: M-3 + M. xanthus (biotic test)</i>								
0	8.00	7.94	1.81	15.6	-1.9772	-4.3341	4.88E-07	40.0
1	7.94	7.99	37.7	23.4	-2.0145	-4.1784	6.41E-07	52.5
3	7.99	8.31	38.2	18.1	-2.0225	-4.2584	5.24E-07	42.9
5	8.31	8.12	23.9	20.2	-2.0499	-3.9105	1.10E-06	89.7
7	8.12	8.03	22.5	12.3	-2.0835	-4.3305	3.85E-07	31.6
10	8.03	8.41	15.1	10.2	-2.1100	-4.4387	2.83E-07	23.1
15	8.41	8.43	13.5	9.7	-2.1342	-4.1366	5.36E-07	43.9
30	8.43	39.6	11.1	7.7	-2.0402	-4.2740	4.85E-07	39.7

precipitation is recorded by a decrease in Ω_{vaterite} and $\text{Ca}_{\text{T(aq)}}$ values, as shown in Fig. 6b and c. Two main precipitation events were observed (Fig. 6a and b). The system stabilized after 15 days, indicating that there was probably not enough bacterial activity to induce another precipitation event.

Spatial-temporal changes of Ω_{vaterite} altered the precipitation rate and morphology of biotic vaterite crystals. The

precipitation of smaller poorly crystallized vaterite crystals surrounding the bacterial cells (first vaterite ring shown in Fig. 4d) occurred at the highest supersaturation, the closest to the bacterium cell wall. As supersaturation decreased, a lower nucleation and growth rate resulted in bigger, better-crystallized vaterite crystals (second vaterite ring). The occurrence of several layers surrounding bacterial cells could indicate a periodic precipitation process favored by

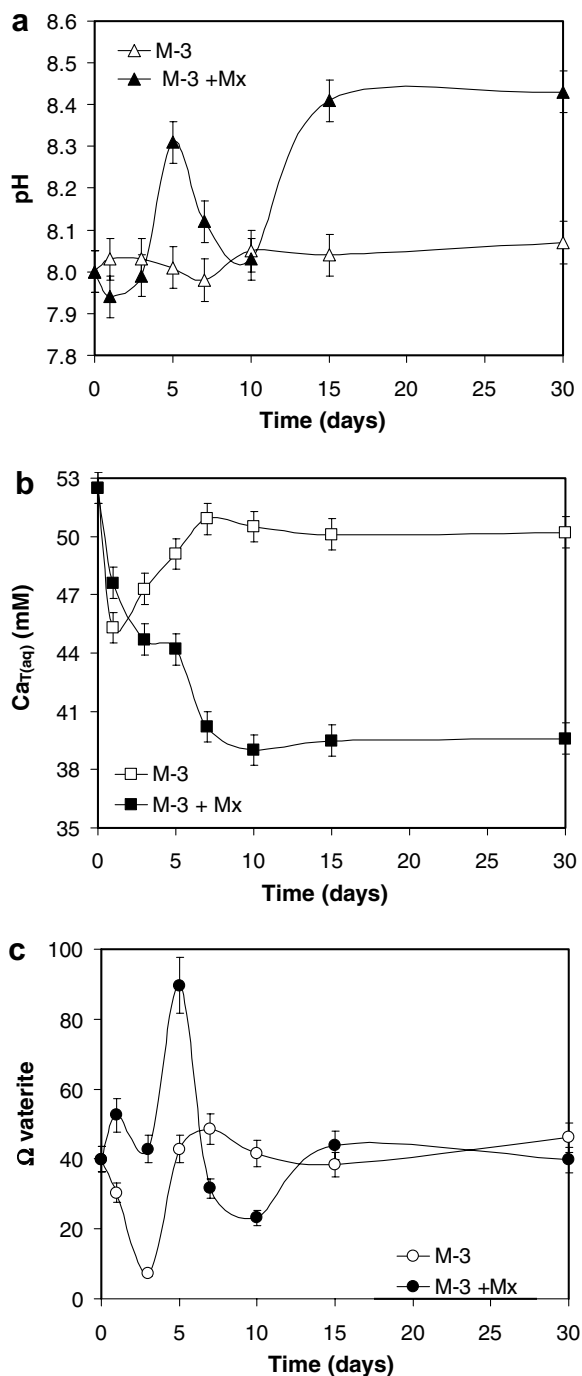


Fig. 6. Time evolution of the (a) pH; (b) total calcium in solution, $Ca_{T(aq)}$; and (c) supersaturation of the medium with respect to vaterite, $\Omega_{vaterite}$, for the biotic experiment: M-3 culture medium inoculated with *M. xanthus* (M-3 + Mx, biotic test) and sterile (M-3, negative biotic control).

the high $\Omega_{vaterite}$ (52.5–89.7) such as that forming Liesegang rings in far-from-equilibrium inorganic systems (Henisch, 1988).

No precipitation was detected during the time course experiment in sterile M-3 culture medium (negative biotic control). The decrease in $\Omega_{vaterite}$ and $Ca_{T(aq)}$ occurring during the first stages of this experiment (Fig. 6b and c) might be related to the adsorption of Ca at negatively

charged xilanol groups on the silica glass Erlenmeyer flask. Limited silica dissolution in the slightly alkaline medium resulting in Ca desorption may explain the subsequent increase in $\Omega_{vaterite}$ and $Ca_{T(aq)}$ until constant values were reached.

Precipitation of calcite and aragonite did not occur in the biotic test experiments (inoculated with *M. xanthus* and sterile—negative biotic control), even though the medium was supersaturated with respect to calcite (~ 331 and ~ 180 , respectively) and with respect to aragonite (~ 240 and ~ 130 , respectively). Such a high supersaturation with respect to all $CaCO_3$ polymorphs could be sustained initially due to the crystallization inhibition effect of organics (Bacto Casitone and/or organic by-products of bacterial activity) (Mullin, 1993; Arp et al., 2001). The precipitation of vaterite at such high supersaturation could be kinetically favored compared with other more stable $CaCO_3$ polymorphs, according to Ostwald's rule of stages (Ogino et al., 1987; Jimenez-Lopez et al., 2001).

In addition to kinetic effects, oriented vaterite crystallization on bacterial cells could be induced by template-directed growth, provoked by electrostatic (ionotropic effect), geometric, or stereochemical affinity (Mann, 2001). These effects would control polymorph selection and promote heterogeneous nucleation of vaterite. Conversely, vaterite formation and stabilization could be due to the adsorption of organic molecules (Bacto Casitone and/or EPS produced by bacterial activity) during the early stages of (nano-sized) vaterite crystallization, thus interrupting the Ostwald rule of stages at one of its intermediate stages (Ogino et al., 1987; Xu et al., 2004; Lakshminarayanan et al., 2005). A third possibility could be a combination of the two previous processes. In order to check these hypotheses and to elucidate the ultimate mechanism leading to bacterial vaterite formation, a detailed TEM and electron diffraction study of vaterite structures was performed. With these analyses we expected to identify: (a) possible preferred orientation of vaterite crystals which may support Mann's model for template-directed growth; (b) existence of nanocrystals with organics at their boundaries making up larger vaterite crystals, which would support an origin of vaterite due to an interruption of the Ostwald rule at an intermediate stage.

3.3. TEM and electron diffraction analysis

TEM observations of cross sections of the biotic vaterite spheroids (Fig. 7A and C) showed that they formed by radial prismatic vaterite crystals that branched as they approached the spheroid edge (Fig. 7D and E). Such branched structure is similar to that of biomimetic fluorapatite (Busch et al., 1999) and calcium carbonate (Cölfen and Qi, 2001) spheroids formed in the presence of organics via a sheaf-of-wheat growth mechanism. This type of spherulitic growth can occur by attachment of prismatic nanocrystals to an already existing crystal of the same phase or an organic particle (e.g., a bacterial cell) that act

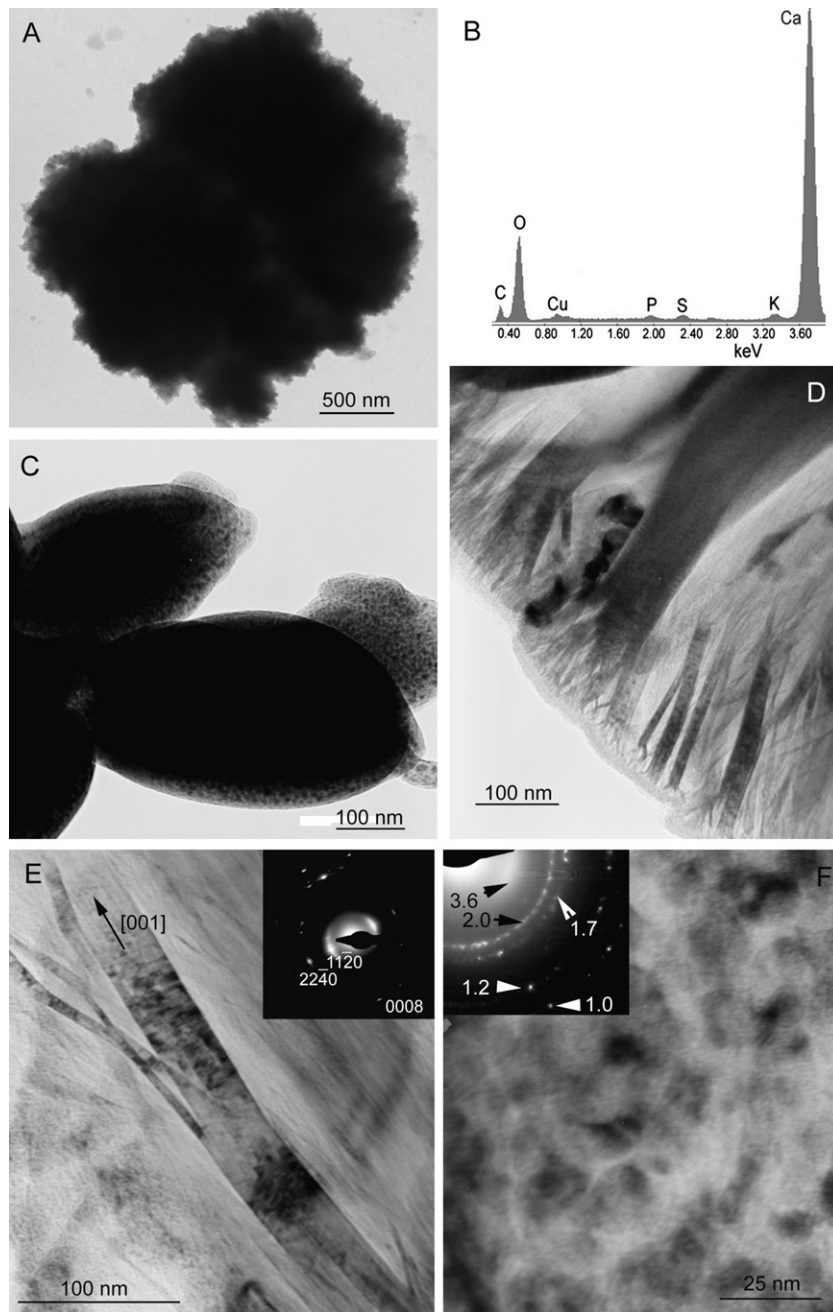


Fig. 7. TEM analysis of biotic vaterite structures. (A) Low magnification photomicrograph of a representative biotic vaterite spherulite; (B) EDS spectrum of the former spherulite; (C) detail of a large spherulite attached to two spherulites with diameter smaller than $1\ \mu\text{m}$ (i.e., smaller than *M. xanthus* cells); (D) higher-magnification of the edge of a large vaterite spherulite showing radial arrangement of branch-like crystals; branching takes place towards the shell edge (lower left) where crystal size decreases substantially; (E) detail of prismatic vaterite crystals in (D); the SAED pattern (inset) shows 1120, 2240, and 0008 reflections, showing orientation of the prism along the *c*-axis, which is oriented normal to the spherulite nucleus (i.e., the bacterium); (F) vaterite crystals in a section tangential to the spherulite edge; the SAED pattern (inset) shows rings corresponding to vaterite main reflections along [0001] zone axis ($hh2\bar{h}0$ and $h0\bar{h}0$ reflections; *d*-spacing in nm); rings show rotation of crystals around their *c*-axis.

as a nucleus. One important characteristic of these spherulites is that they incorporate organics within the porous inorganic framework (Cölfen and Qi, 2001). Note that individual crystals in our biotic vaterite structures were separated by poorly electron absorbent material (Fig. 7D). We assume these areas correspond to the organics of bacterial origin identified by FTIR and thermal analysis. This is consistent with EDS analyses showing the presence of P

and S in biotic vaterite (Fig. 7B), in addition to Ca (vaterite) and Cu (TEM grid). P and S are present in Bacto Casitone, because casein includes S- and P-containing amino acids. S and P are also present in bacterial EPS and cell-walls (e.g., proteins-containing sulfur amino acids, and phospholipids) (Li et al., 2003). Another principal characteristic of the spherulitic biomimetic mesostructures described by Cölfen and Qi (2001) and Busch et al. (1999)

is the marked orientation of the prismatic crystals constituting the spherulites. In our case, the *c*-axis of each vaterite crystal was aligned perpendicular to the spherulite nucleus as shown by selected area electron diffraction (SAED) pattern (Fig. 7E). However, in sections tangential to the vaterite spherulite, [0001] zone axis SAED patterns were ring-like (Fig. 7F) which indicates that there was no clear preferred orientation in the (0001) basal planes [i.e., the *a*- and *b*-axes show a random orientation within the (0001) plane].

The outer edge of some vaterite structures was formed by isolated crystallites, 10–30 nm in diameter (Fig. 8A), embedded in poorly electron absorbent material (organics, as confirmed by EDS analysis). In areas deeper into the spherulite structure, such crystallites aggregate into larger ones (Fig. 8B) forming the grained structure (Fig. 8C) observed on the near-surface of the spherulites (Fig. 4b). Towards the core of the spherulite, a transition to oriented, small prismatic crystals (branch-like aggregates) was observed (Fig. 8D). This latter observation suggest that the nanocrystals present at the spherulite surface aggregate in a crystallographically oriented fashion as growth progresses, thus forming the larger prismatic crystals observed in deeper areas. In fact, high resolution TEM (HRTEM) observations showed that vaterite prisms were formed by nanocrystals that have aggregated in an oriented fashion (Fig. 9). The nanoparticle average size was ~20–30 nm, measured in sections perpendicular to (11 $\bar{2}$ 0), a value similar to that of isolated crystallites shown in Fig. 8A. Such

crystallite size is consistent with analyses of XRD peak broadening [37 ± 10 nm, in sections normal to (11 $\bar{2}$ 0)]. At nanoparticle boundaries there were discontinuities in lattice fringes (Fig. 9C–E), which suggests that nanoparticles were partially surrounded by amorphous (organic) material. Buckling of lattice fringes in a single crystallite (Fig. 9B) and a non-perfect orientation of the aggregated nanocrystals was also observed (Fig. 9C–E). On other areas of the same prism, (11 $\bar{2}$ 0) lattice fringes were observed in contact with domains with (11 $\bar{2}$ 0) \wedge (11 $\bar{2}$ 2) lattice fringes intersecting at an angle of ca. 40° (Fig. 9C and D). These observations demonstrate that a slight missorientation exists between nearby nanocrystallites. Furthermore, abundant edge dislocations interpreted to have formed by imperfectly oriented aggregation of nanocrystals (see following subsection) were also observed (Fig. 9E).

The TEM analysis of abiotic vaterite structures (Fig. 10) showed some morphological/textural differences when compared with the previously described biotic structures. Abiotic spherulites (Fig. 10A) showed radial arrangement of vaterite crystals oriented along the *c*-axis (Fig. 10B). However, this orientation is poorer than the one in biotic vaterite, as shown by speckled rings in the SAED pattern (Fig. 10B). Another main difference with biotic vaterite structures was the presence of calcite along with vaterite in some of the abiotic carbonate structures (SAED pattern in Fig. 10B and C). Vaterite structures were formed by nanocrystals, as in the biotic structures (Fig. 10D). However we observed neither well-formed, oriented prismatic

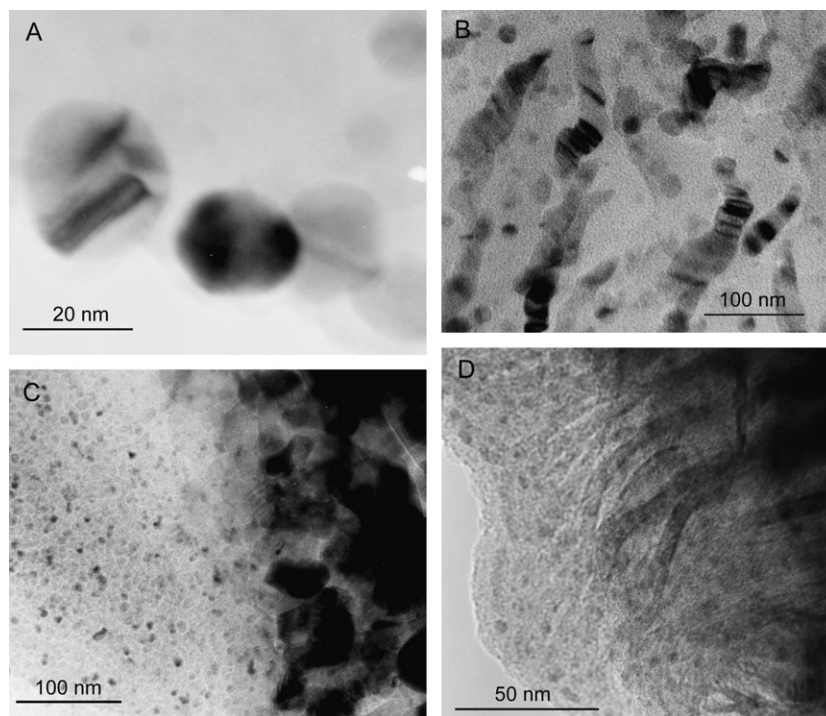


Fig. 8. TEM of biotic vaterite nanocrystals: (A) isolated vaterite nanocrystals embedded in an amorphous, poorly electron absorbent continuous phase (organics) found at the outer edge of spherulites; (B) vaterite nanocrystals aggregated in larger clusters placed beneath the previous isolated nanocrystals; (C) nanocrystals aggregated at the edge of a spherulite (left). The core of the spherulite is towards the right; and (D) cross-section of a bacterial spherulite showing randomly oriented nanocrystals (left) and branch-like prismatic vaterite crystal in a deeper area within the spherulite (right).

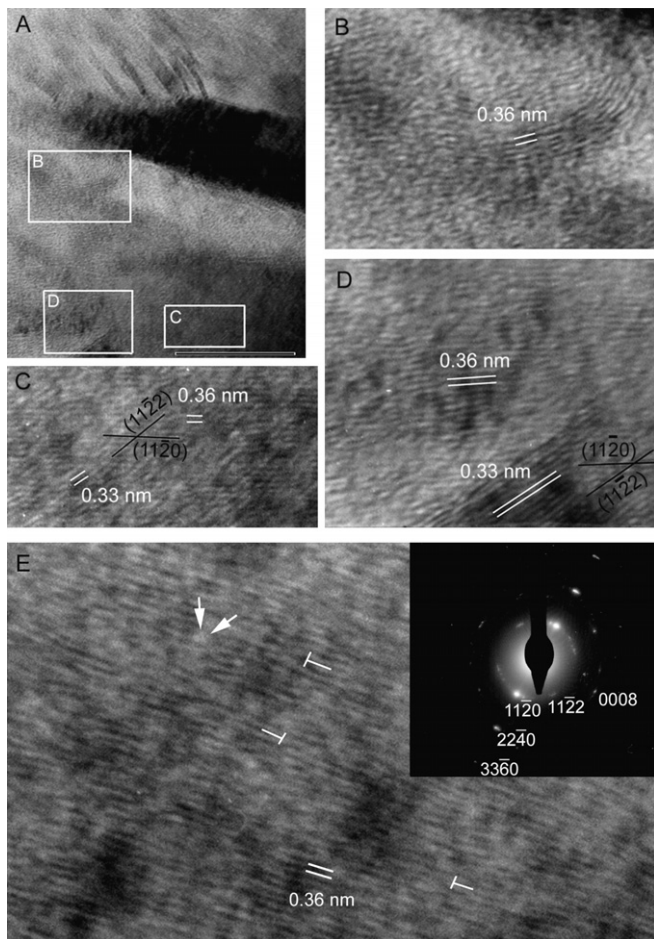


Fig. 9. High resolution TEM of biotic vaterite. (A) Vaterite prisms in a radial section of a spherulite showing selected (squared) areas (bar, 100 nm); (B) $(11\bar{2}0)$ lattice fringe image of vaterite prism; buckling of a crystal edge is observed; (C) contact between two domains in a single vaterite prism showing miss-orientation between $(11\bar{2}0)$ lattice fringes and areas with crossing $(11\bar{2}0)$ and $(11\bar{2}2)$ lattice fringes; (D) detail of domains showing $(11\bar{2}0)$ and $(11\bar{2}2)$ lattice fringes; and (E) $[1\bar{1}00]$ zone axis image of a radially arranged prismatic crystal showing misalignment between $(11\bar{2}0)$ lattice fringes of different nanocrystals (i.e., crystallites). Arrow pair indicates orientation mismatch (ending dislocations) between nearby nanocrystals and non-diffracting material at their boundary. A few examples (three) of edge dislocations interpreted to have formed by imperfectly oriented aggregation are also indicated. SAED pattern (inset) shows orientation of the c -axis normal to the cell-wall (not shown; located on the right). Ellipsoidal diffraction spots corroborate the observed orientation mismatching among nanocrystals.

crystals in deeper areas of the spherulites, nor the branched arrangement of such crystals at the outer edge of the vaterite structures that were observed in the biotic precipitates.

3.4. Origins of bacterial vaterite

Our results suggest that vaterite precipitation is directly related to the high supersaturation reached in both the biotic and abiotic systems. In the latter case (abiotic), such a high supersaturation is reached following NH_3 addition (pH rise) and CO_2 bubbling, while in the former (biotic), the high supersaturation is related to bacterial activity. In

both cases the presence of organic molecules also appears to be crucial for vaterite crystallization and stabilization. While Bacto Casitone is critical in the formation and (partial) stabilization of abiotic vaterite, the bacterium cell walls, EPS as well as the organic by-products of bacterial activity, appear to control biotic vaterite formation and its long-term stabilization in a much more efficient way than Bacto Casitone alone. Bacteria cell walls contain a number of surface functional groups, such as carboxyl, hydroxyl and phosphate sites (Schultze-Lam et al., 1996), while Bacto Casitone, as well as bacterial EPS, include carboxylic and amino functional groups, which are known to promote vaterite crystallization and stabilization (Naka and Chujo, 2001). Organic molecules with these functional groups can either inhibit crystallization when they are in the bulk solution (Mullin, 1993), or promote crystallization when they are adsorbed at the air–liquid or solid–liquid interface, or incorporated in solid structures (Mann, 2001).

By acting as crystallization inhibitors, organics induce precipitation at a high supersaturation (Mullin, 1993), which favors the formation of metastable phases (Clarkson et al., 1992). In our biotic experiments a high supersaturation is reached due to ammonia release associated to bacterial activity and the subsequent pH rise leading to high alkalinity values (Table 1). The latter, in addition to the inhibiting effect of organics, may kinetically favor the formation of nano-sized vaterite crystals. Our study suggests that once nano-sized vaterite crystals have formed, they aggregate in an oriented fashion and incorporate the adsorbed organics at the nanocrystal boundaries. Interestingly, this orientation is much better defined in biotic than in abiotic vaterite structures. The latter probably indicates that the higher amount of organics incorporated in the biotic vaterite spherulites is critical in the formation and stabilization of such oriented structures.

The observed ultrastructural features of our biotic vaterite spherulites appear to be general for biominerals formed by oriented aggregation of nanoparticles (Banfield et al., 2000). According to Penn and Banfield (1998) model for oriented aggregation-based crystal growth, nanometer-sized nuclei are formed, attach stereochemically and aggregate in a crystallographically oriented manner. In some cases, a non-perfect oriented attachment occurs (Banfield et al., 2000), which helps to identify the boundaries between nearby nanoparticles, as was observed in our biotic vaterite structures. Removal of a pair of surfaces is energetically favored. Aggregation is also favored when particles have a lower surface charge, i.e., at pH values close to the isoelectric point. Biotic vaterite precipitation occurs at pH 8–9 (Fig. 6). Note that the isoelectric point (or point of zero charge, PZC) of vaterite is at pH 9.9 (Vdovic and Kralj, 2000). Under such conditions, aggregation might result from attractive forces experienced between uncharged nanoparticles and hydrophobic moieties on organic polymers (Moreau et al., 2004). The latter thus act as crystal “assemblers” (Cölfen and Antonietti, 2005) and are incorporated into the vaterite structures contributing to their stability.

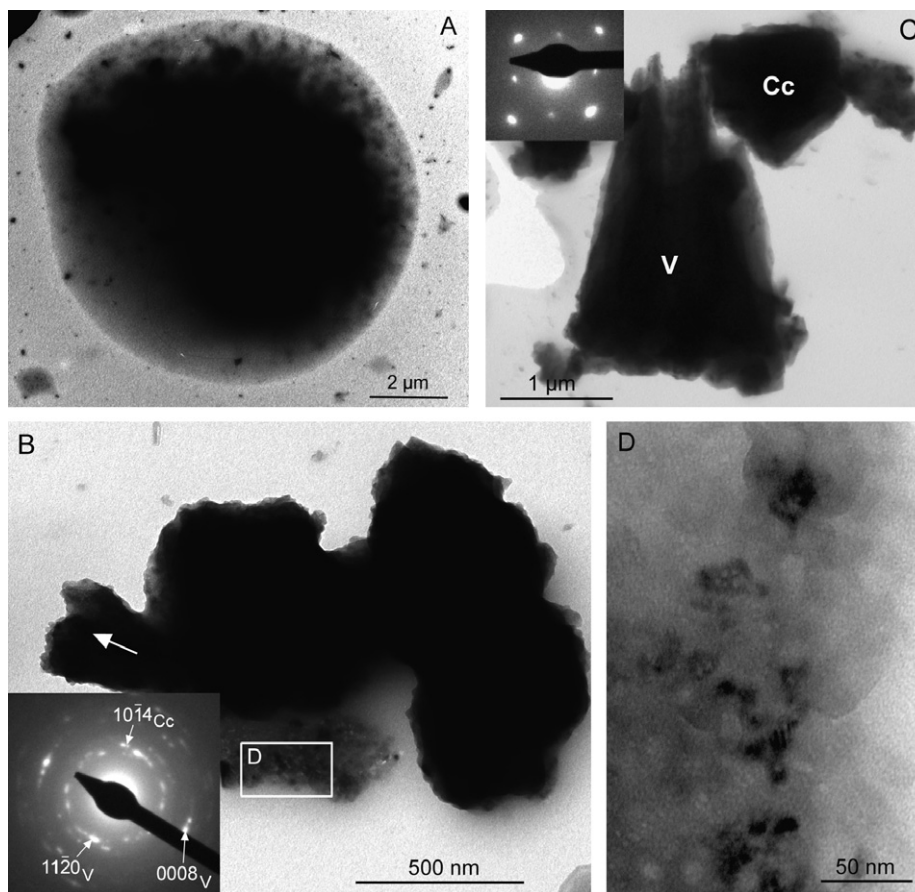


Fig. 10. TEM photomicrographs of abiotic carbonates: (A) vaterite spherulite; (B) aggregate of vaterite spherulites. The SAED pattern (inset) of a broken spherulite (arrow) shows speckled rings indicating a poorly defined orientation along vaterite [0001] zone axis (vaterite c -axis orientation indicated by the arrow in the photomicrograph). Diffraction spots corresponding to calcite ($10\bar{1}4$) planes are also present; (C) Detail of the section of a broken vaterite (V) spherulite and of a calcite (Cc) crystal. The SAED of Cc is shown in inset; and (D) detail of nanocrystal aggregates at the edge of vaterite spherulites in the section marked in (B).

Nanocrystal aggregates may eventually attach to a solid support (EPS or bacterial cell walls) in an oriented manner. This phenomenon is clearly observed in the case of the hollow spherulites formed in our biotic experiments. They display a radial arrangement of oriented prismatic vaterite crystals attached to the bacterial cell walls. Such crystals attach with their c -axis normal to the substrate. This final oriented attachment requires that some electrostatic, geometrical or stereochemical affinity exist between the (0001) faces of vaterite and the organic support (Mann, 2001). The observed lack of preferred orientation along the vaterite (0001) planes in biotic structures (i.e., crystals are rotated around the c -axis), in addition to the reported precipitation of calcite and Mg-calcite around *M. xanthus* cells (González-Muñoz et al., 2000; Rodríguez-Navarro et al., 2003; Ben Chekroun et al., 2004), rule out a geometric or stereochemical matching among this bacterium cell-wall macromolecular functional groups and vaterite crystals. Conversely, the high Ca density of vaterite (0001) planes enables a high electrostatic affinity between these positively charged planes and the negatively charged functional groups of the bacterium cell-wall. Thus, nanocrystals

will preferentially attach to the cell-wall with their c -axis normal to this substratum. In the case of EPS the same rationale may apply. Amino acids in the medium where abiotic vaterite spherulites developed could play a role (although less effective) directing the assembly of nanocrystals in an oriented manner. Alternatively, it is suggested that a vaterite crystal may act as a nucleus for the oriented attachment of successive crystals following the model proposed by Busch et al. (1999) for self-assembled spherulitic growth. The latter mechanism could operate both in the biotic and abiotic experiments, thus explaining the eventual formation of spherulites lacking an organic nucleus/core.

Thus, it appears that vaterite crystallization is promoted by kinetic effects, while the formation of the highly oriented vaterite structures is due to thermodynamic effects. The kinetic effects are associated with the high supersaturation, resulting from bacterial activity and the inhibiting role of organics (i.e., Bacto Casitone and by-products of bacterial metabolism), all of which lead to high reaction rates. The thermodynamic effect is linked to energy minimization due to electrostatic affinity, i.e., ionotropic effect, and crystal attachment at equally oriented faces.

4. Conclusions

Our analyses suggest that vaterite precipitation occurs at a very high supersaturation resulting from bacterial activity (biotic experiment) or from the addition of NH_3 and $\text{CO}_2(\text{g})$ (abiotic experiment). This high supersaturation is achieved because of crystallization inhibition associated with the organics that are originally present in the culture medium (abiotic test), in addition to those (EPS) produced by bacterial activity (biotic tests). At such a high supersaturation 3D nucleation of vaterite nanoparticles occurs in the microenvironment surroundings of the bacterial cells. Oriented aggregation of nanoparticles then occurs and leads to the incorporation of organics into vaterite structures. Incorporation of organics within vaterite leads to highly insoluble structures and contributes to vaterite stabilization.

Valuable information regarding the bacterial/inorganic origin of natural vaterites on Earth and elsewhere, may be related to the complex inner structure and ultrastructure of biotic vaterite spheroids: i.e., degree of crystal orientation, amount of organic matter, presence of various shells, and hollow core–shell structure. Considering that bacteria have been related to human pathological calcification (Mc Lean et al., 1989), vaterite being found in human gallstones (Sutor and Wooley, 1968) and aortic valves (Kanakis et al., 2001), our results may help determine whether such vaterite pathological concretions are of bacterial origin, which is critical to the design of adequate medical treatments. However, a purely morphological (size and shape) analysis of such vaterite structures can not be used as an unambiguous biosignature since similar (spherulitic) morphologies are obtained by biotic and abiotic routes. Nonetheless, the presence of organics appears to be a prerequisite for vaterite formation and stabilization.

Finally, our results, as well as those of other studies (Rivadeneira et al., 1991; Giralt et al., 2001; Groth et al., 2001; Warren et al., 2001; Braissant et al., 2002, 2003; Caccchio et al., 2003; Hammes et al., 2003; Rivadeneira et al., 2006), demonstrate that bacterial vaterite precipitation is not strain-specific and is much more common than was previously thought.

Acknowledgments

We thank J.F. Banfield, F. Nieto, A. Putnis, L. Warren, E.H. Oelkers, and three anonymous referees for valuable comments and suggestions. We also thank Dr. Arias-Peñalver for his indications for culturing and working with *M. xanthus*. The personnel of the Centro de Instrumentación Científica (CIC; Granada University) assisted with the TGA/DSC, TEM and FESEM analyses. Some of the FTIR, XRD, and FESEM analyses were carried out by E. Ruiz-Agudo and F.J. Carrillo-Rosua. This research was financed by Spanish Ministerio de Educación y Ciencia Grants MAT2001-3074, MAT 2005-03994, MAT2006-05411, BOS2001-3285, and REN2003-07375, Research

Groups RNM 179 and CVI 103, and two Ramón y Cajal Program fellowships (C.J.L. and A.R.N.). C.J.L. also thank project CGL2004-03910. Editing of the English manuscript was done by M. Bettini.

Associate editor: Eric H. Oelkers

References

- Agarwal, P., Berglund, K.S., 2003. In situ monitoring of calcium carbonate polymorphs during batch crystallization in the presence of polymeric additives using Raman spectroscopy. *Crystal Growth Des.* **3**, 941–946.
- Aizenberg, J., Lambert, G., Weiner, S., Addadi, L., 2002. Factors involved in the formation of amorphous and crystalline calcium carbonate: a study of an ascidian skeleton. *J. Am. Chem. Soc.* **124**, 32–39.
- Albright, J.N., 1971. Vaterite stability. *Am. Miner.* **56**, 620–624.
- Ariani, A.P., Wittmann, K.J., Franco, E., 1993. A comparative study of static bodies in Mysid crustaceans—evolutionary implications of crystallographic characteristics. *Biol. Bull.* **185**, 393–404.
- Arp, G., Reiner, A., Reitner, J., 2001. Photosynthesis-induced biofilm calcification and calcium concentration in Phanerozoic oceans. *Science* **292**, 1701–1704.
- Balz, M., Therese, H.A., Li, J., Gutmann, J.S., Kappl, M., Nasdala, L., Hofmeister, W., Butt, H.J., Tremei, W., 2005. Crystallization of vaterite nanowires by the cooperative interaction of tailor-made nucleation surfaces and polyelectrolites. *Adv. Funct. Mater.* **15**, 683–688.
- Banfield, J.F., Nealson, K.H., 1997. *Geomicrobiology: Interactions between microbes and minerals*. Reviews in Mineralogy, vol. 35. Mineralogical Society of America, Washington, DC.
- Banfield, J.F., Welch, S.A., Zhang, H., Ebert, T.T., Penn, R.L., 2000. Aggregation-based crystal growth and microstructure development in natural iron oxyhydroxide biomineralization products. *Science* **289**, 751–754.
- Bassi, N., Delfavero, G., Meggiato, T., Scaloni, P., Ghiro, S., Molin, M., Pilotto, A., Vigneri, S., Savarino, V., Mela, G.S., Dimario, F., 1994. Are morphology and composition of gallstones related—an X-ray-diffraction study. *Curr. Ther. Res. Clin. Exp.* **55**, 1169–1175.
- Belcher, A.M., Wu, X.H., Christensen, R.J., Hansma, P.K., Stucky, G.D., Morse, D.E., 1996. Control of crystal phase switching and orientation by soluble mollusk-shell proteins. *Nature* **381**, 56–58.
- Ben Chekroun, K., Rodríguez-Navarro, C., González-Muñoz, M.T., Arias, J.M., Cultrone, G., Rodríguez-Gallego, M., 2004. Precipitation and growth morphology of calcium carbonate induced by *Myxococcus xanthus*: implications for recognition of bacterial carbonates. *J. Sedimentary Res.* **74**, 868–876.
- Ben Omar, N., Entrena, M., González-Muñoz, M.T., Arias, J.M., Huertas, F., 1994. The effects of pH and phosphate on the production of struvite by *Myxococcus xanthus*. *Geomicrobiol. J.* **12**, 81–90.
- Benton, Y.K., Gross, S., Heller, L., 1963. Some unusual minerals from the “mottled zone” complex, Israel. *Am. Miner.* **48**, 924–930.
- Beveridge, T.J., Graham, L.L., 1991. Surface layers of bacteria. *Microbiol. Rev.* **55**, 684–705.
- Bogren, H.G., Mutvei, H., Renberg, G., 1995. Scanning electron-microscope studies of human gallstones after plasma-etching. *Ultrastruct. Pathol.* **19**, 447–453.
- Braissant, O., Verrecchia, E.P., Aragno, M., 2002. Is the contribution of bacteria to terrestrial carbon budget greatly underestimated?. *Naturwissenschaften* **89** 366–370.
- Braissant, O., Cailleau, G., Dupraz, C., Verrecchia, A.P.J., 2003. Bacterially induced mineralization of calcium carbonate in terrestrial environments: the role of exopolysaccharides and amino acids. *J. Sedimentary Res.* **73**, 485–490.
- Busch, S., Dolhaine, H., DuChesne, A., Heinz, S., Hochrein, O., Laeri, F., Podebrad, O., Vietze, U., Weiland, T., Kniep, R., 1999. Biomimetic

- morphogenesis of fluorapatite-gelatin composites: fractal growth, the question of intrinsic electric fields, core/shell assemblies, hollow spheres and reorganization of denaturated collagen. *Eur. J. Inorg. Chem.* **1999**, 1643–1653.
- Cacchio, P., Ercole, C., Capuccio, G., Lepidi, A., 2003. Calcium carbonate precipitation by bacterial strains isolated from a limestone cave and from a loamy soil. *Geomicrobiol. J.* **29**, 85–98.
- Chen, S.F., Yu, S.H., Jiang, J., Li, F., Liu, Y., 2006. Polymorph discrimination of CaCO₃ mineral in an ethanol/water solution: Formation of complex vaterite superstructures and aragonite rods. *Chem. Mater.* **18**, 115–122.
- Clarkson, J.R., Price, T.J., Adams, C.J., 1992. Role of metastable phases in the spontaneous precipitation of calcium carbonate. *J. Chem. Soc. Faraday Trans.* **88**, 243–249.
- Cole, W.F., Kroone, B., 1959. Carbonate minerals in hydrated portland cement. *Nature* **184**, 57.
- Cölfen, H., Antonietti, M., 1998. Crystal design of calcium carbonate microparticles using double-hydrophilic block copolymers. *Langmuir* **14**, 582–589.
- Cölfen, H., Qi, L., 2001. A systematic examination of the morphogenesis of calcium carbonate in the presence of a double-hydrophilic block copolymer. *Chem. Eur. J.* **7**, 106–116.
- Cölfen, H., Antonietti, M., 2005. Mesocrystals: Inorganic superstructures made by highly parallel crystallization and controlled alignment. *Angew. Chem. Int. Ed.* **44**, 5576–5591.
- Dalas, E., Klepetsanis, P., Koutsoukos, P.G., 1999. The overgrowth of calcium-carbonate on poly(vinyl chloride-co-vinyl acetate-co-maleic acid). *Langmuir* **15**, 8322–8327.
- David, A.W., Grimes, C.B., Isely, J.J., 1994. Vaterite sagittal otoliths in hatchery-reared juvenile Red Drums. *Prog. Fish Culturist* **56**, 301–303.
- Decho, A.W., 2000. Microbial biofilms in intertidal systems: an overview. *Continental Shelf Res.* **20**, 1257–1273.
- Dennis, J.E., Xiao, S.Q., Agarwal, M., Fink, D.J., Heuer, A.H., Caplan, A.I., 1996. Microstructure of matrix and mineral components of eggshells from White Leghorn chickens (*Gallus Gallus*). *J. Morphol.* **228**, 287–306.
- Dickinson, S.R., McGrath, K.M., 2001. Quantitative determination of binary and tertiary calcium carbonate mixtures using powder X-ray diffraction. *Analyst* **126**, 1118–1121.
- DiMasi, E., Olszta, M.J., Patel, V.M., Gower, L.B., 2003. When is template directed mineralization really template directed? *Crystal Eng. Comm.* **5**, 346–350.
- DuFresne, E.R., Anders, F., 1962. On the retention of primordial noble gases in the Pesyanoe meteorite. *Geochim. Cosmochim. Acta* **26**, 251–262.
- Dupont, L., Portemer, F., Figlarz, M., 1997. Synthesis and study of a well crystallized CaCO₃ vaterite showing a new habitus. *J. Mater. Chem.* **7**, 797–800.
- Dworkin, M., Kaiser, D., 1993. *Myxobacteria II*. American Society for Microbiology, Washington, DC.
- Ehrlich, H.L., 2002. *Geomicrobiology*, fourth ed. Marcel Dekker, New York.
- Falini, G., Albeck, S., Weiner, S., Addadi, L., 1996. Control of aragonite or calcite polymorphism by mollusk shell macromolecules. *Science* **271**, 67–69.
- Falini, G., Fermani, S., Gazzano, M., Ripamonti, A., 1998. Oriented crystallization of vaterite in collagenous matrices. *Chem. A Eur. J.* **4**, 1048–1052.
- Falini, G., Fermani, S., Gazzano, M., Ripamonti, A., 2000. Polymorphism and architectural crystal assembly of calcium carbonate in biologically inspired polymeric matrices. *J. Chem. Soc. Dalton Trans.*, 3983–3987.
- Falini, G., Fermani, S., Ripamonti, A., 2002. Crystallization of calcium carbonate salts into beta-chitin scaffold. *J. Inorg. Biochem.* **91**, 475–480.
- Falini, G., Fermani, S., Vanzo, S., Miletic, M., Zaffino, G., 2005. Influence on the formation of aragonite and vaterite by otolith macromolecules. *Eur. J. Inorg. Chem.*, 162–167.
- Fan, Y., Wang, R., 2005. Submicrometer-sized vaterite tubes formed through nanobubble-templated crystal growth. *Adv. Mater.* **17**, 2384–2388.
- Ferris, F.G., Phoenix, V., Fujita, Y., Smith, R.W., 2003. Kinetics of calcite precipitation induced by ureolytic bacteria at 10 and 20 degrees C in artificial groundwater. *Geochim. Cosmochim. Acta* **68**, 1701–1710.
- Friedman, G.M., Schultz, D.J., 1994. Precipitation of vaterite (CaCO₃) during oil-field drilling. *Miner. Mag.* **58**, 401–408.
- Friedman, G.M., Schultz, D.J., Guo, B., Sanders, J.E., 1993. Vaterite (an uncommon polymorph of CaCO₃): occurrences in boreholes demonstrate unexpected longevity. *J. Sedimentary Petrol.* **63**, 663–664.
- Frumkin, A., Shimron, A., Rosebaum, J., 2003. Radiometric dating of the Siloam Tunnel, Jerusalem. *Nature* **425**, 169–171.
- Fujita, Y., Redden, G.D., Ingram, J.C., Cortez, M.M., Ferris, F.G., Smith, R.W., 2004. Strontium incorporation into calcite generated by bacterial ureolysis. *Geochim. Cosmochim. Acta* **68**, 3261–3270.
- Gehrke, N., Cölfen, H., Pinna, N., Antonietti, M., Nassif, N., 2005. Superstructures of calcium carbonate crystals by oriented attachment. *Crystal Growth Des.* **5**, 1317–1319.
- Giralt, S., Julia, R., Klerkx, J., 2001. Microbial biscuits of vaterite in Lake Issyk-Kul (Republic of Kyrgyzstan). *J. Sedimentary Res.* **71**, 430–435.
- González-Muñoz, M.T., BenOmar, N., Martínez-Cañamero, M., Rodríguez-Gallego, M., López Galindo, A., Arias, J.M., 1996. Struvite and calcite crystallization induced by cellular membranes of *Myxococcus xanthus*. *J. Crystal Growth* **163**, 434–439.
- González-Muñoz, M.T., BenChekroun, K., BenAboud, A., Arias, J.M., Rodríguez-Gallego, M., 2000. Bacterially induced Mg–calcite formation: role of Mg²⁺ in development of crystal morphology. *J. Sedimentary Res.* **70**, 559–564.
- González-Muñoz, M.T., Fernández-Luque, B., Martínez-Ruiz, F., Ben Chekroun, K., Arias, J.M., Rodríguez-Gallego, M., Martínez-Cañamero, M., deLinares, C., Paytan, A., 2003. Precipitation of barite by *Myxococcus xanthus*: possible implications for the biogeochemical cycle of barium. *Appl. Environ. Microbiol.* **69**, 5722–5725.
- Grasby, S.E., 2003. Naturally precipitating vaterite (μ-CaCO₃) spheres: unusual carbonates formed in an extreme environment. *Geochim. Cosmochim. Acta* **67**, 1659–1666.
- Grassmann, O., Müller, G., Löbmann, P., 2002. Organic–inorganic hybrid structure of calcite crystalline assemblies grown in a gelatin hydrogel matrix: relevance to biomineralization. *Chem. Mater.* **14**, 4530–4535.
- Grassmann, O., Neder, R.B., Putnis, A., Löbmann, P., 2003. Biomimetic control of crystal assembly by growth in an organic hydrogel network. *Am. Miner.* **88**, 647–652.
- Grassmann, O., Löbmann, P., 2004. Biomimetic nucleation and growth of CaCO₃ in hydrogels incorporating carboxylate groups. *Biomaterials* **25**, 277–282.
- Groth, I., Schumann, P., Laiz, L., Sanchez-Moral, S., Cañaveras, J.C., Saiz-Jimenez, C., 2001. Geomicrobiological study of the Grotta dei Cervi, Porto Badisco, Italy. *Geomicrobiol. J.* **18**, 241–258.
- Hall, A., Taylor, J.D., 1971. Occurrence of vaterite in gastropod eggshells. *Miner. Mag.* **38**, 521–522.
- Hammes, F., Boon, N., de Villiers, J., Verstratet, W., Siciliano, S.D., 2003. Strain-specific ureolytic microbial calcium carbonate precipitation. *Appl. Environ. Microbiol.* **69**, 4901–4909.
- Han, Y.S., Hadiko, G., Fuji, M., Takahashi, M., 2006. Crystallization and transformation of vaterite at controlled pH. *J. Crystal Growth* **289**, 269–274.
- Henisch, H.K., 1988. *Crystals in Gels and Liesegang Rings*. Cambridge Univ. Press, Cambridge.
- Ichikawa, K., Shimomura, N., Yamada, M., Ohkubo, N., 2003. Control of calcium carbonate polymorphism and morphology through biomimetic mineralization by means of nanotechnology. *Chem. Eur. J.* **9**, 3235–3241.
- Jada, A., Verraes, A., 2003. Preparation and microelectrophoresis characterization of calcium carbonate particles in the presence of anionic polyelectrolyte. *Colloids Surf. A Physicochem. Eng. Aspects* **219**, 7–15.

- Jimenez-Lopez, C., Caballero, E., Huertas, F.J., Romanek, C.S., 2001. Chemical, mineralogical and isotope behavior, and phase transformation during the precipitation of calcium carbonate minerals from intermediate ionic solution at 25 °C. *Geochim. Cosmochim. Acta* **65**, 3219–3231.
- Kanakis, J., Malkaj, P., Petroheilos, J., Dalas, E., 2001. The crystallization of calcium carbonate on porcine and human cardiac valves and the antimicrobial effect of sodium alginate. *J. Crystal Growth* **223**, 557–564.
- Klug, H.P., Alexander, L.E., 1954. *X-ray Diffraction Procedures for Polycrystalline and Amorphous Materials*. Wiley, New York.
- Kralj, D., Brečević, L., Kontrec, J., 1997. Vaterite growth and dissolution in aqueous solution III. Kinetics of transformation. *J. Crystal Growth* **177**, 248–257.
- Lakshminarayanan, R., Chi-Jin, E.O., Loh, X.J., Kini, R.M., Valiyaveetil, S., 2005. Purification and characterization of vaterite-inducing peptide, pelovaterin, from the eggshells of *Pelodiscus sinensis* (Chinese soft-shelled turtle). *Biomacromolecules* **6**, 1429–1437.
- Li, Y., Sun, H., Ma, X., Lu, A., Lux, R., Zusman, D., Shi, W., 2003. Extracellular polysaccharides mediate pilus retraction during social motility of *Myxococcus xanthus*. *Proc. Natl. Acad. Sci. USA* **100**, 5443–5446.
- Liang, P., Shen, Q., Zhao, Y., Zhou, Y., Wei, H., Lieberwirth, I., Huang, Y., Wang, D., Xu, D., 2004. Petunia-shaped superstructures of CaCO₃ aggregates modulated by modified chitosan. *Langmuir* **20**, 10444–10448.
- Lippmann, F., 1973. *Sedimentary Carbonate Minerals*. Springer-Verlag, Berlin.
- Lowenstam, H.A., Abbott, D.P., 1975. Vaterite: a mineralization product of the hard tissues of a marine organism (Ascidacea). *Science* **188**, 363–365.
- Lowenstam, H.A., Weiner, S., 1989. *On Biomineralization*. Oxford Univ. Press, Oxford.
- Lucas, D., Andrews, J.E., 1996. A re-examination of reported lacustrine vaterite formation in Holkham Lake, Norfolk, U.K. *J. Sedimentary Res.* **66**, 474–476.
- Malkaj, P., Dalas, E., 2004. Calcium carbonate crystallization in the presence of aspartic acid. *Crystal Growth Des.* **4**, 721–723.
- Mann, S., 2001. *Biomineralization: Principles and Concepts in Bioinorganic Materials Chemistry*. Oxford Univ. Press, Oxford.
- Mann, S., Heywood, B.R., Rajam, S., Birchall, J.D., 1988. Controlled crystallization of CaCO₃ under stearic-acid monolayers. *Nature* **334**, 692–695.
- Mann, S., Heywood, B.R., Rajam, S., Walker, J.B.A., 1991. Structural and stereochemical relationships between Langmuir monolayers and calcium carbonate nucleation. *J. Phys. D Appl. Phys.* **24**, 154–164.
- Manoli, F., Kanakis, J., Malkaj, P., Dalas, E., 2002. The effect of amino acids on the crystal growth of calcium carbonate. *J. Crystal Growth* **236**, 363–370.
- Mayer, F.K., Weineck, E., 1932. Die Verbreitung des Kalziumkarbonat im Tierreich unter besonderer Berücksichtigung der Wirbellosen. *Z. Naturwiss.* **66**, 199–222.
- McConnel, J.D.C., 1960. Vaterite from Ballycraigy, Larne, Northern Ireland. *Miner. Mag.* **32**, 534–544.
- Mc Lean, R.J.C., Nickel, J.C., Beveridge, T.J., Costerton, J.W., 1989. Observations of the ultrastructure of infected kidney stones. *J. Med. Microbiol.* **29**, 1–7.
- McSwain, B.S., Irvine, R.L., Hausner, M., Wilderer, P.A., 2005. Composition and distribution of extracellular polymeric substances in the aerobic flocs and granular sludge. *Appl. Environ. Microbiol.* **71**, 1051–1057.
- Meyer, H.J., 1969. Struktur und Fehlordnung des Vaterits. *Z. Kristallogr.* **128**, 183–212.
- Mitchell, A.C., Ferris, F.G., 2005. The coprecipitation of Sr into calcite precipitates induced by bacterial ureolysis in artificial groundwater: Temperature and kinetic dependence. *Geochim. Cosmochim. Acta* **69**, 4199–4210.
- Mitchell, A.C., Ferris, F.G., 2006. The influence of *Bacillus pasteurii* on the nucleation and growth of calcium carbonate. *Geomicrobiol. J.* **23**, 213–226.
- Moreau, J.W., Webb, R.I., Banfield, J.F., 2004. Ultrastructure, aggregation-state, and crystal growth of biogenic nanocrystalline sphalerite and wurtzite. *Am. Miner.* **89**, 950–960.
- Mullin, J.W., 1993. *Crystallization*, third ed. Butterworth, Heinemann, Oxford.
- Naka, K., Chujo, Y., 2001. Control of crystal nucleation and growth of calcium carbonate by synthetic substrates. *Chem. Mater.* **13**, 3245–3259.
- Ogino, T., Suzuki, T., Sawada, K., 1987. The formation and transformation mechanism of calcium carbonate in water. *Geochim. Cosmochim. Acta* **51**, 2757–2767.
- Oliveira, A.M., Farina, M., Ludka, I.P., Kachar, B., 1996. Vaterite, calcite, and aragonite in the otoliths of 3 species of piranha. *Naturwissenschaften* **83**, 133–135.
- Palchik, N.A., Moroz, T.N., 2005. Polymorph modifications of calcium carbonate in gallstones. *J. Crystal Growth* **283**, 450–456.
- Penn, R.L., Banfield, J.F., 1998. Imperfect oriented attachment: dislocation generation in defect-free nanocrystals. *Science* **281**, 969–971.
- Plummer, L.N., Busenberg, E., 1982. The solubilities of calcite, aragonite and vaterite in CO₂-H₂O solutions between 0 °C and 90 °C, and an evaluation of the aqueous model for the system CaCO₃-CO₂-H₂O. *Geochim. Cosmochim. Acta* **46**, 1011–1040.
- Rajam, S., Heywood, B.R., Walker, J.B.A., Mann, S., Davey, R.J., Birchall, J.D., 1991. Oriented crystallization of CaCO₃ under compressed monolayers. I. Morphological studies of mature crystals. *J. Chem. Soc. Faraday Trans.* **87**, 727–734.
- Rautaray, D., Ahmad, A., Sastry, M., 2003. Biosynthesis of CaCO₃ crystals of complex morphology using a fungus and an actinomycete. *J. Am. Chem. Soc.* **125**, 14656–14657.
- Riding, R., 2000. Microbial carbonates: the geological record of calcified bacterial-algal mats and biofilms. *Sedimentology* **47** (Suppl. 1), 179–214.
- Rivadeneira, M.A., Delgado, R., Quesada, E., Ramos-Cormenzana, A., 1991. Precipitation of calcium-carbonate by *Deleya-Halophila* in media containing NaCl as sole salt. *Curr. Microbiol.* **22**, 185–190.
- Rivadeneira, M.A., Martín-Algarra, A., Sánchez-Navas, A., Martín-Ramos, D., 2006. Carbonate and phosphate precipitation by *Chromohalobacter marismortui*. *Geomicrobiol. J.* **23**, 89–101.
- Rodriguez-Navarro, C., Rodriguez-Gallego, M., BenChekroun, K., Gonzalez-Muñoz, M.T., 2003. Conservation of ornamental stone by *Myxococcus xanthus*-induced carbonate biomineralization. *Appl. Environ. Microbiol.* **69**, 2182–2193.
- Rudolf, J., Cölfen, H., 2003. Superstructures of temporarily stabilized nanocrystalline CaCO₃ particles: morphological control via water surface tension variation. *Langmuir* **20**, 991–996.
- Sawada, K., 1997. The mechanisms of crystallization and transformation of calcium carbonates. *Pure Appl. Chem.* **69**, 921–928.
- Sánchez-Moral, S., Cañaveras, J.C., Laiz, L., Saiz-Jimenez, C., Bedoya, J., Luque, L., 2003. Biomediated precipitation of calcium carbonate metastable phases in hypogean environments: a short review. *Geomicrobiol. J.* **20**, 491–500.
- Signorelli, S., Peroni, C., Camaiti, M., Fratini, F., 1996. The presence of vaterite in bonding mortars of marble inlays from Florence Cathedral. *Miner. Mag.* **60**, 663–665.
- Schultze-Lam, S., Fortin, D., Davis, B.S., Beveridge, T.J., 1996. Mineralization of bacterial surfaces. *Chem. Geol.* **132**, 171–181.
- Shen, Q., Wei, H., Wang, L., Zhou, Y., Zhao, Y., Zhang, Z., Wang, D., Xu, G., Xu, D., 2005a. Crystallization and aggregation behaviors of calcium carbonate in the presence of poly(vinylpyrrolidone) and sodium dodecyl sulfate. *J. Phys. Chem. B* **109**, 18342–18347.
- Shen, Q., Chen, Y., Wei, H., Zhao, Y., Wang, D., Xu, D., 2005b. Suspension effect of poly(styrene-ran-methacrylic acid) latex particles on crystal growth of calcium carbonate. *Crystal Growth Des.* **5**, 1387–1391.

- Sondi, I., Matiječić, E., 2001. Homogeneous precipitation of calcium carbonates by enzyme catalyzed reaction. *J. Colloid Interface Sci.* **238**, 208–214.
- Spanos, N., Koutsoukos, P.G., 1998. The transformation of vaterite to calcite—effect of the conditions of the solutions in contact with the mineral phase. *J. Crystal Growth* **191**, 783–790.
- Sutor, D.J., Wooley, S.E., 1968. Gallstone of unusual composition: calcite, aragonite and vaterite. *Science* **159**, 1113–1114.
- Takahashi, K., Doi, M., Kobayashi, A., Taguchi, T., Onoda, A., Okamura, T., Yakamoto, H., Ueyama, N., 2004. Formation of 6-, 7-, or 8-membered ring intra-side-chain NH-O hydrogen bond toward Ca-binding oxyanion in poly(allylaminocarboxylate) ligands stabilizes CaCO₃ vaterite crystals. *J. Crystal Growth* **263**, 552–563.
- Tong, H., Ma, W., Wang, L., Wan, P., Hu, J., Cao, L., 2004. Control over crystal shape, size and aggregation of calcium carbonate via L-aspartic acid inducing process. *Biomaterials* **25**, 3923–3929.
- Ueyama, N., Takahashi, K., Omoda, A., Okamura, T., Yamamoto, H., 2002. Tight binding of poly(carboxylate) ligand to calcium carbonate with intramolecular NH-O hydrogen bond. *Macromol. Symp.* **186**, 129–134.
- Vdovic, N., Kralj, D., 2000. Electrokinetic properties of spontaneously precipitated calcium carbonate polymorphs: the influence of organic substances. *Colloids Surf. Physicochem. Eng. Aspects* **161**, 499–505.
- Vecht, A., Ireland, T.G., 2000. The role of vaterite and aragonite in the formation of pseudo-biogenic carbonate structures: implications for Martian exobiology. *Geochim. Cosmochim. Acta* **64**, 2719–2725.
- Walsh, D., Lebeau, B., Mann, S., 1999. Morphosynthesis of calcium carbonate (vaterite) microsponges. *Adv. Mater.* **11**, 324–328.
- Wang, J.J., Xu, Y.Z., Zhao, Y., Huang, Y.P., Wang, D.J., Jiang, L., Wu, J.G., Xu, D.F., 2003. Morphology and crystalline characterization of abalone shell and mimetic mineralization. *J. Crystal Growth* **252**, 367–371.
- Warren, L.A., Maurice, P.A., Parmar, N., Ferris, F.G., 2001. Microbially mediated calcium carbonate precipitation: implications for interpreting calcite precipitation and for solid-phase capture of inorganic contaminants. *Geomicrobiol. J.* **18**, 93–115.
- Williams, D.H., Fleming, T., 1989. *Spectroscopic Methods in Organic Chemistry*, fourth ed. McGraw-Hill, London.
- Wingender, J., Neu, T., Flemming, H.C., 1999. *Microbial Extracellular Polymeric Substances: Characterization, Structure and Function*. Springer, Berlin.
- Wolery, T.J. 1992. EQ3/6, A Software Package for Geochemical Modeling of Aqueous Systems. Version 7.0. University of California, Livermore.
- Wright, C.G., Rouse, R.C., Weinberg, A.G., Johnsson, L.G., Hubbard, D.G., 1982. Vaterite otoconia in 2 cases of otoconial membrane dysplasia. *Ann. Otol. Rhinol. Laryngol.* **91**, 193–199.
- Xie, A.J., Shen, Y.H., Zhang, C.Y., Yuan, Z.W., Zhu, X.M., Yang, Y.M., 2005. Crystal growth of calcium carbonate with various morphologies in different amino acid systems. *J. Crystal Growth* **285**, 436–443.
- Xu, X., Han, J.T., Cho, K., 2004. Formation of amorphous calcium carbonate thin films and their role in biomineralization. *Chem. Mater.* **16**, 1740–1746.